PNAS RESEARCH ARTICLE | ENGINEERING OPEN ACCESS

SonoTransformers: Transformable acoustically activated wireless microscale machines

Zhiyuan Zhang[a], Zhan Shi[a], and Daniel Ahmed[a,1]

Edited by Yihui Zhang, Tsinghua University, Beijing, China; received August 26, 2023; accepted December 22, 2023 by Editorial Board Member Yonggang Huang

Shape transformation, a key mechanism for organismal survival and adaptation, has gained importance in developing synthetic shape-shifting systems with diverse applications ranging from robotics to bioengineering. However, designing and controlling microscale shape-shifting materials remains a fundamental challenge in various actuation modalities. As materials and structures are scaled down to the microscale, they often exhibit size-dependent characteristics, and the underlying physical mechanisms can be significantly affected or rendered ineffective. Additionally, surface forces such as van der Waals forces and electrostatic forces become dominant at the microscale, resulting in stiction and adhesion between small structures, making them fracture and more difficult to deform. Furthermore, despite various actuation approaches, acoustics have received limited attention despite their potential advantages. Here, we introduce "SonoTransformer," the acoustically activated micromachine that delivers shape transformability using preprogrammed soft hinges with different stiffnesses. When exposed to an acoustic field, these hinges concentrate sound energy through intensified oscillation and provide the necessary force and torque for the transformation of the entire micromachine within milliseconds. We have created machine designs to predetermine the folding state, enabling precise programming and customization of the acoustic transformation. Additionally, we have shown selective shape transformable microrobots by adjusting acoustic power, realizing high degrees of control and functional versatility. Our findings open new research avenues in acoustics, physics, and soft matter, offering new design paradigms and development opportunities in robotics, metamaterials, adaptive optics, flexible electronics, and microtechnology.

acoustics | soft matter | wireless micromachines | metamaterials | shape transformation

Significance

Shape transformation, a key mechanism observed in organisms for survival and adaptation, has seen tremendous growth in synthetic shape-shifting systems. However, developing transformable machines at the microscale remains a fundamental challenge. Furthermore, despite various actuation approaches, acoustics have received limited attention. Here, we present "SonoTransformers," acoustically activated transformable micromachines. We found that applied sound energy can be trapped and amplified on the soft hinge, causing deformation of the entire micromachine within milliseconds. Multiple hinges are designed to predetermine the folding state, enabling precise programming and customization of the acoustic transformation. With adjustable acoustic power, we showcase controlled and selective shape transformable microrobots, promising versatile applications in flexible electronics, medicine, and microengineering, offering new design paradigms and opportunities for future developments.

Numerous organisms large and small shift their shapes in order to effectively survive and thrive in complex natural environments. For instance, armadillos curl their bodies into balls to protect themselves from danger, while frilled lizards spread their umbrella-like collar membranes in threat and mating displays. On the microscopic level, unicellular organisms like amoebae extend pseudopods for locomotion and feeding, while a vorticella can contract its spasmoneme within milliseconds (1, 2) (Fig. 1*A*). Such shape transformations are facilitated by a complex interplay network of soft and rigid architectures, which are characterized by adaptability, flexibility, conformability, energy efficiency, and safety. Drawing inspiration from nature's solutions can serve to inspire innovative artificial systems capable of shape-shifting (3–7), the potential applications of which span fields as diverse as robotics, wearable devices, materials science, and bioengineering.

Shape transformation in artificial systems has been implemented by means of several actuation methods, such as mechanical pushes (8, 9), pressurized fluids (10–12), shape memory polymers and alloys (13–15), liquid crystal elastomers (16, 17), and conductive polymers (18–20). Researchers have also utilized a range of external stimuli and fields, including chemical gradients (21–24), light (25–29), heat (30–32), humidity (33), electric, and magnetic fields (34–41) to actuate small untethered machines. However, most existing machines are limited to centimeter-sized or millimeter-sized structures, which precludes their use in miniaturized microscale machines. These pioneering studies also exhibit certain limitations; for example, most actuation methods are often slow (1 to 150 s), resulting in lower deformation speeds. Although electromagnetic actuation can be regarded as instantaneous (41, 42), sophisticated pre-programming is needed to produce micromachines compatible with these methods, such as predesigned magnetic moments, multiple layers, and multistep processes. In addition, the underlying physical mechanisms governing their operation can be significantly affected or rendered ineffective when scaled down.

As materials and structures are scaled down to the microscale, they often exhibit size-dependent characteristics (43, 44), leading to mechanical variations that are difficult to predict and control during shape transformation. Additionally, surface forces such as

Author contributions: Z.Z. and D.A. designed research; Z.Z., Z.S., and D.A. performed research; Z.Z. and Z.S. contributed new reagents/analytic tools; Z.Z., Z.S., and D.A. analyzed data; and Z.Z., Z.S., and D.A. wrote the paper.

The authors declare no competing interest.

This article is a PNAS Direct Submission. Y.Z. is a guest editor invited by the Editorial Board.

[1]To whom correspondence may be addressed. Email: dahmed@ethz.ch.

This article contains supporting information online at https://www.pnas.org/lookup/suppl/doi:10.1073/pnas.2314661121/-/DCSupplemental.

Published January 30, 2024.

van der Waals forces and electrostatic forces become dominant at the microscale (45, 46), leading to increased stiction and adhesion between small structures. This makes them more prone to fracture and more challenging to deform. Surprisingly, acoustics, despite offering exciting prospects for transformable micromachines, have received little attention. Acoustics presents a promising avenue for transformable micromachines as they enable miniaturization at micro and nanoscales, simplified design and rapid prototyping, and remote and wireless operation (47–58), as well as ultrafast and reversible transformation in milliseconds. Leveraging acoustics could potentially overcome some of the aforementioned challenges and pave the way for innovative advancements in this field.

In this study, we demonstrate acoustically activated transformable micromachines that can change their shapes in milliseconds (30 to 500 ms) upon the application of an acoustic field and rebound to their original state when the field is deactivated, as illustrated in Fig. 1*B*. These micromachines comprise multiple geometric interconnected acoustic-deformable microbeams, which are serially constructed of rigid links and soft hinges with different stiffnesses. When exposed to an acoustic field, the soft hinge oscillates and induces shape-shifting of the entire microbeam within milliseconds. The force and torque necessary for this shifting are provided by the asymmetrical acoustic radiation force and streaming caused by the oscillation of the soft hinge. We demonstrate the remarkable

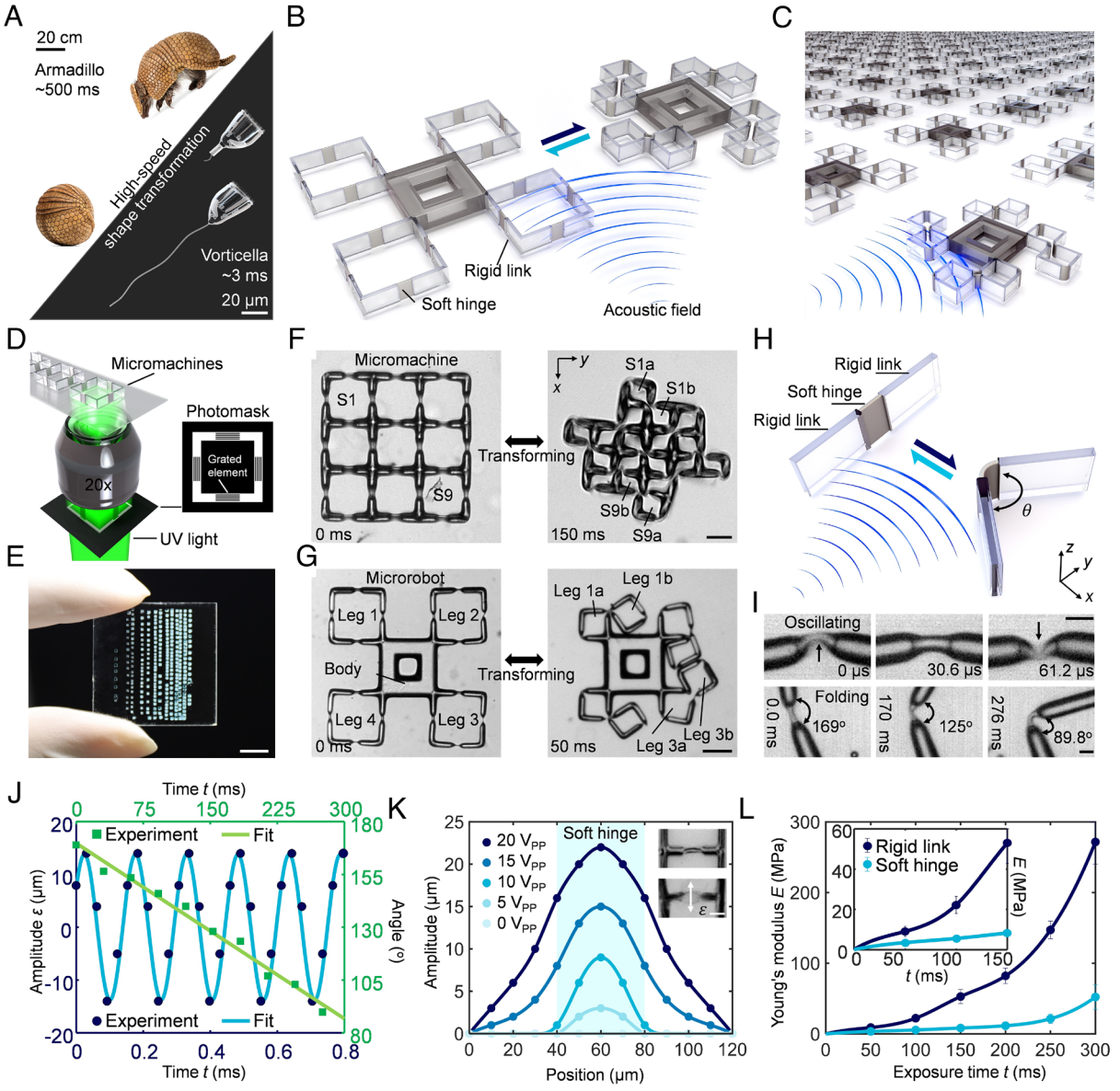

Fig. 1. Acoustically actuated shape transformation. (*A*) Shape transformation occurs across different scales in nature represented by an armadillo and a vorticella. (*B*) Schematic of an untethered soft micromachine and its high-speed, reversible shape transformation in an acoustic field. (*C* and *D*) The schematic of high throughput micromachine array and photopolymerization setup. *Inset* shows the photomask with blank and grated elements. (*E*) An image shows hundreds of soft micromachines fabricated on a chip. (Scale bar, 5 mm.) (*F*) An untethered microscale auxetic contracts in both length and width from its original shape to a fully folded shape in 150 ms. (Scale bar, 100 μm.) (*G*) A quadrupedal microrobot folds its outer four-square legs in 50 ms. (Scale bar, 100 μm.) (*H*) Illustration of the folding mechanism of an acoustic-deformable microbeam composed of a soft hinge positioned between two rigid links. (*I*) Image sequences demonstrate the oscillation of the soft hinge and folding of the entire microbeam captured by a high-speed camera. (Scale bar, 20 μm.) (*J*) Plots of the sinusoidal oscillation of the soft hinge and linear folding of the entire microbeam against time. (*K*) Plots of the oscillation amplitude along the acoustic-deformable microbeam at different positions according to the acoustic excitation voltage. *Inset* shows the oscillation of the clamped-clamped microbeam. (Scale bar, 50 μm.) (*L*) Plots of stiffnesses of the soft hinge and rigid link according to the duration of UV exposure. *Inset* shows a zoomed-in subplot of the 0 to 150 ms exposure range.

capacity of acoustic activation to trigger auxetic, isomeric, and selective shape transformation of micromachines depending on their geometric parameters. These results offer different design paradigms with a wide range of applications on the microscale, encompassing soft robotics, flexible electronics, intelligent metamaterials, adaptive optics, advanced micro-medicines, and beyond.

Results

Design and Characterization of Transformable Microscale Machines. We fabricated prototypes of the acoustic-transformable micromachines using a custom-built ultraviolet (UV) photopolymerization technique (as shown in Fig. 1 *C* and *D*), which utilizes a photomask and a photosensitive hydrogel mixture on a glass substrate. The designed patterns of micromachines are projected into the hydrogel mixture as the UV light passes through the photomask, resulting in the polymerization of the hydrogel mixture (59–61). To achieve varying stiffnesses and thicknesses in the micromachine, we designed the photomask with blank and grated elements that alter the local exposure intensity. Blank elements result in full polymerization, producing a relatively rigid region, while grated elements enable partial polymerization, resulting in a soft and flexible region (*SI Appendix*, Fig. S1). Here, we designed and fabricated micromachines with varying hinges that comprise 10 to 70% of the total microbeam length of 140 to 200 μm, and 25 to 50% of the 25 to 40 μm microbeam thickness, but a uniform height of 50 μm in the z-direction. These machines were created using a UV exposure time ranging from 80 to 150 ms. Our fabrication process can produce a single batch of up to 500 micromachines in just 3 min (Fig. 1*E*). Further details on our fabrication process can be found in the *Materials and Methods*.

We characterized these shape-transformable micromachines in an experimental setup that includes a piezo transducer (PZT) bonded next to an acoustic chamber to generate an acoustic wavefield, with both components mounted on a glass slide. The transient dynamics of micromachines were studied using an inverted microscope with a high-speed camera. We applied acoustic fields with voltage amplitudes of 10 to 60 V_{PP} and operating frequencies between 5.5 and 6.5 kHz, which closely match the resonance frequency of the transducer-glass system. Further details are provided in the *Materials and Methods*.

The soft hinge of the acoustic-deformable microbeam serves as a crucial component in our transformable micromachines, enabling their shape-shifting capabilities. As sound propagates through the liquid medium and encounters the microscale auxetic micromachine, it contracts in both length and width, achieving its fully folded shape in 30 to 200 ms (Movie S1). A representative example of the micromachine is illustrated in Fig. 1*F*: the left square geometry of the micro auxetic denoted as S1 undergoes a transformation that results in the two smaller squares labeled S1a and S1b. Similarly, as shown in Fig. 1*G*, a quadrupedal microrobot demonstrates selective folding of its outer four square-shaped legs, which leads to shape transformation and division of Leg 1 into smaller squares (Leg1a and Leg1b), completed in 50 ms (Movie S2). This dynamic and selective folding is controlled by acoustic voltage, which can be modulated by an external function generator, allowing the microstructures to exhibit a walking gait. Upon switching the acoustic field off, both the micromachine and microrobot swiftly revert to their original shapes (*SI Appendix*, Fig. S2).

To gain further insights into the mechanism underlying the shape transformation (Fig. 1*H*), we observed the dynamics of acoustic-deformable microbeams in an acoustic field through high-speed microscopy. As shown in Fig. 1*I*, our observations unveil a fascinating phenomenon: when the microbeam is clamped at both ends and subjected to an acoustic field, the soft hinge exhibits periodic oscillations (Fig. 1*J*). We found that the sound field concentrates on the soft hinge region, amplifying its oscillation amplitude about five times more than the rigid link (Fig. 1*K* and Movie S3). Injection of tracer microparticles into the liquid revealed the fast oscillations of the soft hinge to create microvortices in the surrounding liquid. When ends of the microbeam are not clamped but have damping elements arising from the viscous fluid, friction, and interconnect effect from other beams, termed the "damped-damped" condition, we observed that the oscillation of the soft hinge-induced rotational motion of the rigid link, which in turn, initiated folding of the microstructure (Fig. 1*I* and Movie S4). The angle between the two rigid links linearly decreases, as depicted in Fig. 1*J*, which is attributed to the torque resulting primarily from the difference in stiffnesses between the rigid link and soft hinge.

We performed a series of experiments to optimize a single unit of the acoustic-deformable microbeam, varying the dimensions of the soft hinge (thickness and length) with the goal of facilitating efficient transformation. We found that reducing the thickness of the soft hinge by 50% (from 25 to 12.5 μm) led to a 63% (from 27 to 44 μm) increase in the oscillation amplitude (ε) of the clamped-clamped microbeam at 59 μm length and 22.5 V_{PP}. Similarly, increasing the length of the soft hinge by 80% (from 95 to 171 μm) resulted in a substantial 56% (from 39 to 61 μm) amplification of the oscillation amplitude of the microbeam at 12.5 μm thickness and 22.5 V_{PP} (*SI Appendix*, Fig. S3). Next, we investigated the folding response time of the nine-square micromachines with varying thicknesses and lengths of the soft hinge. We found that as the thickness of the soft hinge narrowed from 25 to 7 μm while maintaining a consistent length at 20 μm, the response time reduced by 91% (from 915 to 81 ms) under acoustic excitation of 6.5 kHz and 45 V_{PP} (*SI Appendix*, Fig. S4). Conversely, as the length of the soft hinge increased from 10 to 60 μm, while its thickness remained constant at 12.5 μm, the response time decreased by 75% (from 475 to 117 ms). This is attributed to the fact that a thinner and longer soft hinge results in a micromachine with relatively lower rigidity. Consequently, the soft hinge can generate larger acoustic forces, leading to more pronounced folding.

Furthermore, we observed that microbeams fabricated with twice the UV exposure time, from 150 to 300 ms, exhibited a significant decrease in oscillation amplitude by 51% (from 39 to 19 μm) at 12.5 μm thickness, 59 μm length, and 22.5 V_{PP}, which can be attributed to the increased stiffness (*SI Appendix*, Fig. S3). Fig. 1*L* shows the Young's modulus of the acoustic-deformable microbeam increasing against the UV exposure time, measured using an atomic force microscope (AFM) (see *SI Appendix*, *Text S1* and Fig. S5 for details). The results indicate that longer UV exposure times during fabrication notably increase the stiffness of the entire microbeam, especially in microstructures fabricated for over 150 ms. Moreover, at high exposures, the stiffness differential between the rigid link and the soft hinge is substantially greater. The wide range of options for modulating stiffnesses, 50 to 270 MPa for the link and 10 to 50 MPa for the hinge, provides exciting new possibilities for designing and programming transformable micromachines and microrobots.

The variable-stiffness design enables the oscillation and folding of acoustic-deformable microbeams. To describe the dynamic behavior of the entire microbeam in response to acoustic excitation, we developed an approximated linearized model represented by

$$\Delta(x,t) = \sum_{i=1}^{n} \frac{\boldsymbol{F}(x,t)}{E_i I_i} \boldsymbol{N}(x) \boldsymbol{q}_i(t), \ (i = 1, 2, 3, \ \ldots\ldots, n), \quad [1]$$

where $\Delta(x,t)$ is a time-varying deflection of the microbeam at position x along its long axis. $\boldsymbol{F}(x,t)$ denotes the acoustic forces acting on this microbeam, which primarily consist of the acoustic radiation force F_{Rad} and the acoustic streaming force F_{St}. The acoustic radiation force is calculated as $\left|F^i_{\mathrm{Rad}}\right| = \int_{\Omega_i} \frac{2\alpha I_i(x,y)}{c}$, correlating with the absorption coefficient α, the temporal average intensity I of the acoustic wave at a given location, and the speed of the sound in the microbeam c, where i denotes the ith composing element of the microbeam and Ω is the integral domain of the microbeam's surface. Furthermore, the acoustic streaming force is represented as $\left|F^i_{\mathrm{St}}\right| \approx \int_{\Omega_i} \tilde{\alpha}\boldsymbol{v}_0^2 \exp(-2\tilde{\alpha}r)$, where $\tilde{\alpha}$ is the acoustic attenuation coefficient, $\boldsymbol{v}_0$ is the characteristic source velocity amplitude, and r is the propagation distance of the sound wave (62–69). The Young's modulus of each element is represented by E_i, and $I_i = \frac{ha_i^3}{12}$ is the moment of inertia, where h and a_i are the height and thickness of the i th element's cross-section, respectively. $N(x)$ is the mode function matrices of the microbeam which is governed by the beam's boundary conditions. The generalized coordinate vector $\boldsymbol{q}^i(t) = q_c^i + q_w^i(t)$ combines the constant parameter q_c^i and the time-varying parameter $q_w^i(t)$, providing a comprehensive representation of the microbeam's total time-varying displacement. The model aids in quantifying the displacement of the microbeam and supports a theoretical understanding of its dynamic behavior, influenced by factors including its boundary conditions, acoustic excitation, and structural design. This model further suggests that reducing the hinge thickness, increasing the hinge length, and identifying appropriate UV exposure times are the key factors in maximizing the oscillation amplitude and achieving efficient transformation, which is consistent with the results of characterisation experiments. The model can be adapted to more microbeam configurations and acoustic excitation conditions, such as multiple soft hinges, different boundary conditions, and variable acoustic propagation directions and angles, which will facilitate the design of new acoustic-transformable micromachines. Detailed theoretical development, verification, and simulations of the model are provided in *SI Appendix*, *Text S2* and Fig. S6.

Versatile Shape Transformation of Micromachines. To design various types of acoustic-transformable micromachines, we created acoustic-deformable microbeams with straight, curved, and wedge-shaped soft hinges, as shown in Fig. 2*A*. An oscillating straight hinge causes folding of the microbeam. However, due to its symmetric design, the microbeam can fold in both directions. By contrast, an oscillating curved hinge unfolds and extends the microbeam in the opposite direction. Similarly, a specialized asymmetric wedge-shaped hinge can fold the microbeam in a predetermined direction (*SI Appendix*, Fig. S7).

Micromachines incorporating these respective hinges exhibited different behaviors when acoustically actuated. The four-square micromachines, constructed from straight microbeams, contract upon acoustic activation, as illustrated in Fig. 2 *B* and *C*. Conversely, micromachines composed of curved microbeams extend when subjected to acoustic stimulation, shown in Fig. 2*D* and Movie S5. As these microstructures initiate folding or unfolding, they start to rotate around their center cross (x). When folding, the auxetic structure rotates clockwise, and when unfolding, it rotates counterclockwise. The torque driving these rotations can be attributed to the asymmetric positioning of soft hinges in the acoustic field, which produces an unbalanced force when subject to acoustic streaming and radiation forces (*SI Appendix*, Fig. S8 and Movie S6). In addition, as the deformable microbeams are interconnected, any torque applied to one will affect the others. Thus, the resultant net force and net torque cause the micromachines to undergo transformation with a negative Poisson's ratio of around −1 (refer to *SI Appendix*, *Text S3* and Figs. S9 and S10 for calculation method and results). These micromachines possess a elastic modulus significantly smaller than their shear modulus. Consequently, when subjected to an acoustic field, they exhibit consistent and stable auxetic transformation, while maintaining resistance to shear deformation (see *SI Appendix*, *Text S4* and Table S1 for optimization details of these auxetic micromachines).

Fig. 2 *E* and *F* demonstrate the push-pull transformation of a micromachine incorporating both straight and curved acoustic-deformable microbeams. When we activate the acoustic field, different parts of the micromachine extend and contract simultaneously (Movie S5). The combined use of different microbeams allows diverse designs of acoustic-transformable micromachines. We have also developed a T-shaped micromachine that can undergo isomeric transformation (Fig. 2*G*). This capability is achieved through the symmetric placement of soft hinges: Each hinge produces an unbalanced force and torque, and these simultaneous forces coming from different directions cause isomeric transformation. To control the folding direction, we incorporated the asymmetric wedge-shaped soft hinge into the design. This specialized hinge generates a net force in a predetermined direction; specifically, a T-shaped micromachine with a left wedge-shaped hinge deforms outward into a "concave" shape (Fig. 2*H* and Movie S7) while one with a right wedge-shaped hinge folds inward into a "convex" shape (Fig. 2*I* and Movie S7). Through this strategic design of hinge configuration, we have effectively engineered the micromachine to exhibit predictable and targeted transformation behavior, supported by our numerical simulations (*SI Appendix*, Fig. S11).

Selective Shape Transformation of Microrobots. To show the selective shape transformation capacity of micromachines by adjusting the acoustic excitation voltage, we have developed quadrupedal microrobots modeled after a tetrapod consisting of a central bulky body and four surrounding legs, as shown in Fig. 3 *A* and *B*. These legs are constructed using various incorporations of straight and curved acoustic-deformable microbeams. Fig. 3*A* shows a microrobot with four square-shaped legs designed with straight microbeams of different hinge lengths. The microrobot's shape is selectively transformable, as shown in Fig. 3*C*. For excitation voltages below 30 V_{PP}, the microrobot retains its original shape. At 40 V_{PP}, the leg with the longest hinge undergoes folding. When the voltage is further increased to 45 V_{PP}, leg 2 folds while leg 1 remains folded. Finally, when the voltage reaches approximately 50 V_{PP}, leg 3 folds with folded legs 1 and 2. Leg 4, which contains the shortest hinge, does not exhibit folding within the current acoustic excitation (Movie S2). Fig. 3*D* and *SI Appendix*, Fig. S12 shows the dynamic and flexible shape transformation process when adjusting the acoustic excitation voltage. The folding sequence of the microrobot's legs corresponds to the characterization and model analysis of the straight microbeams. As the length of the soft hinges increases, the oscillation becomes easier to induce, thereby requiring lower voltages to initiate folding. This tunability enables us to achieve addressable and programmable shape transformation, highlighting its potential for developing sophisticated and multifunctional microrobots.

We also designed a microrobot consisting of a pair of square-shaped legs with straight hinges and a pair of folded-square-shaped legs with curved hinges arranged diagonally (Fig. 3*B*). Remarkably,

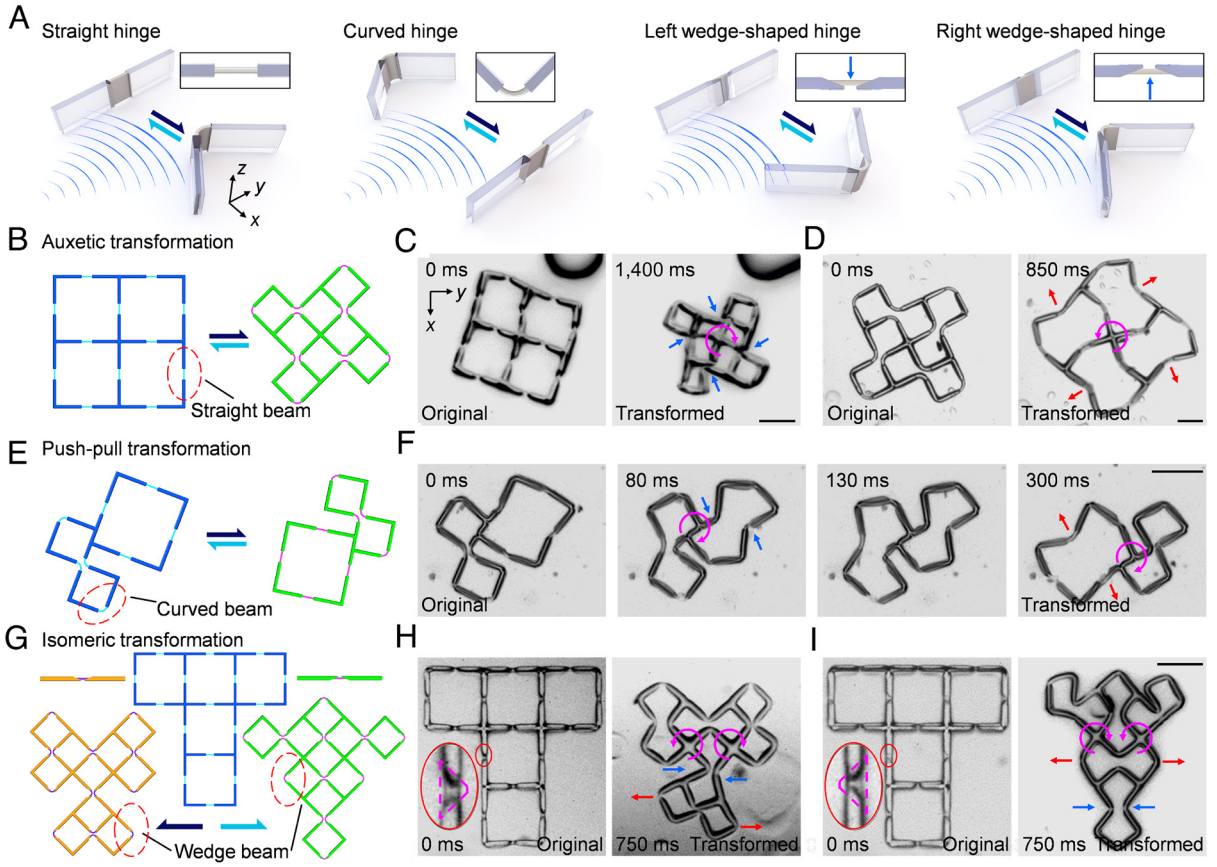

Fig. 2. Versatile shape transformation demonstrated by various soft micromachines. (*A*) Four types of acoustic-deformable microbeams and their deformed shapes with an acoustic activation. *Insets* show the top view of microbeams. The blue arrows demonstrate the predetermined folding directions of the wedge-shaped soft hinges, respectively. (*B*) Bilateral auxetic transformation. (*C*) A four-square micromachine constructed from straight acoustic-deformable microbeams folds into its full-folded shape. (*D*) An inverse four-square micromachine constructed from curved acoustic-deformable microbeams is extended to its full-extended shape. Blue and red arrows, respectively, denote the folding and unfolding behavior of the microbeams. Magenta curved arrows show the rotation direction of the center cross of the micromachine. (*E* and *F*) Push–pull transformation showcased by a micromachine constructed from both straight and curved acoustic-deformable microbeams. Upon acoustic activation, the folded structure extends when the extended structure folds. (*G*) Isomeric transformation showcased by T-shaped micromachines. (*H*) A T-shaped micromachine with the left wedge microbeam transforms toward a "concave" shape. (*I*) A T-shaped micromachine with the right wedge microbeam transforms toward a "convex" shape. (*B*), (*E*), and (*G*) are schematic illustrations of the corresponding shape transformation. (Scale bar [for all optical images], 100 μm.)

when subjected to acoustic stimulation, the microrobot displays rotational motion (Fig. 3*E* and Movie S8), which can be attributed to the net torque generated by its asymmetric structure. We observed a significant increase in the rotational speed with higher acoustic excitation voltages, which increased around 13 times when increasing the voltage from 20 to 50 V_{PP}. For voltages below 20 V_{PP}, the microrobot exhibits a low rotational speed, ranging from 0 to 30 rpm, while retaining its original shape. As the voltage increases to 30 V_{PP}, the four legs exhibit dynamic shape changes between folding and unfolding during rotation. We assume that this is because the applied acoustic forces are similar to the elastic strain energy, resulting in a dynamic balance. When the excitation voltage exceeds 45 V_{PP}, the acoustic forces are larger than the elastic strain energy and result in the full-folded shape of all the four legs, causing a faster rotational speed of around 400 rpm at 52.5 V_{PP} (see *SI Appendix*, Fig. S13 for the rotational speed graph). Additionally, when the leg transforms into different reconfigurations, the microrobot exhibits a reverse rotation (*SI Appendix*, Fig. S14). By using these acoustic-deformable microbeams as the foundational structural module, a broad range of microrobots can be designed with various choices in structural configurations, geometric dimensions, and stiffnesses (see *SI Appendix*, Fig. S15 for more robotic designs).

Discussion

The interaction between sound waves and soft matter, in particular materials of different stiffnesses, remains largely unexplored. In our study, we present acoustically activated transformable soft micromachines. These micromachines incorporate deformable soft microbeams that allow them to change shape in milliseconds upon the application of an acoustic field, as well as to revert to their original state equally rapidly when the field is deactivated. Our simulation and theoretical studies further confirmed this fundamental new shape-transforming mechanism. It merits mention that these micromachines exhibit remarkable reliability and adaptability. Adopting extreme geometric designs such as curved links, point hinges, block links, and broken portions, these soft micromachines still achieve shape transformation (*SI Appendix*, Fig. S16).

The development of versatile deformable microbeams and shape-transformable micromachines paves the way for exciting advancements in multiple scientific domains. From a physics perspective, they offer an exciting opportunity to explore acoustic interactions with soft matter, allowing for the exploration of, for example, oscillation modes and synchronization effects. In the field of microdevices and microfluidics, integrating our micromachines into chip platforms facilitates the use of such platforms in drug delivery, object loading,

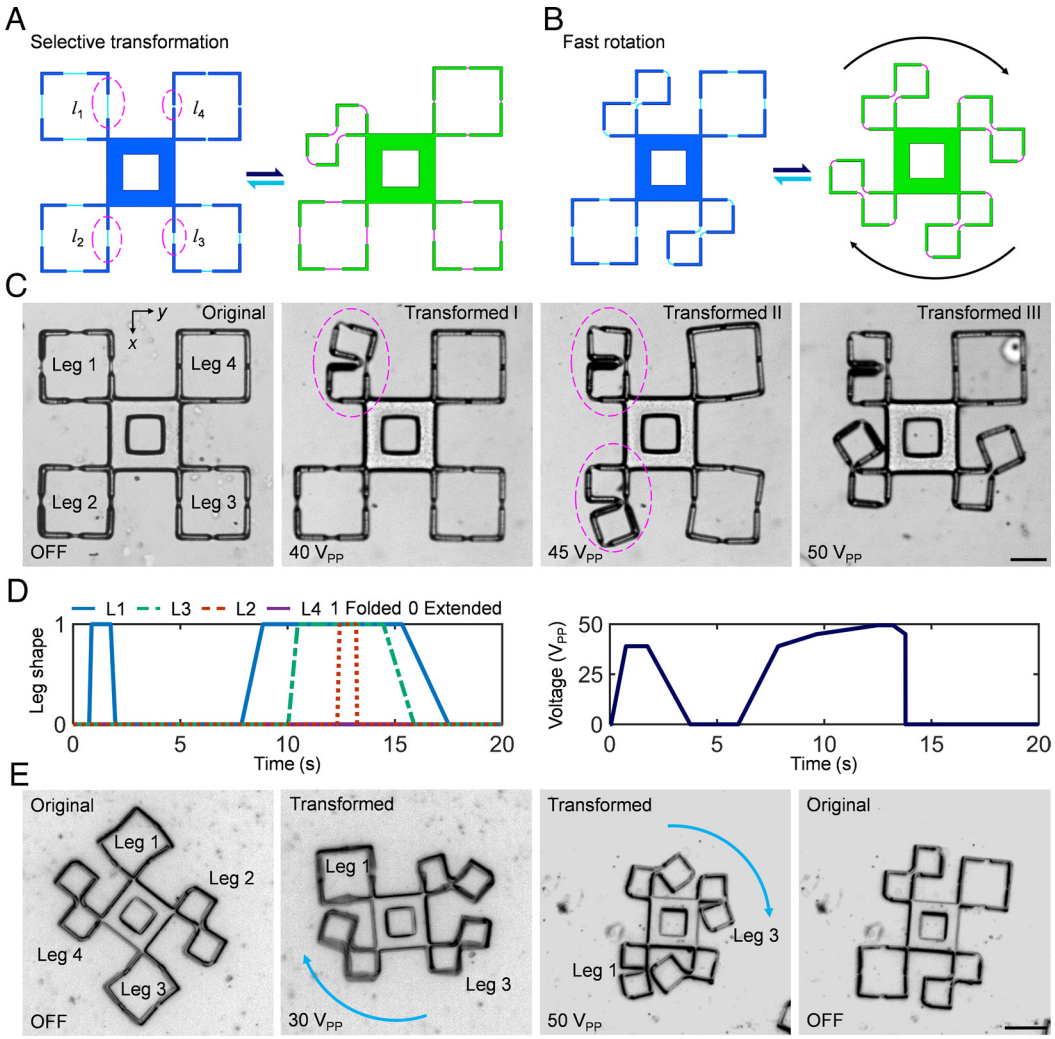

Fig. 3. Selective shape transformation tuned by acoustic excitation voltages. (*A*) Selective transformation of a quadrupedal microrobot with square-shaped legs constructed from straight microbeams with different hinge lengths, namely, 46.2, 33.0, 19.8, and 6.60 μm. (*B*) Fast rotation of a microrobot constructed from straight and curved microbeams with diagonally positioned extended legs and folded legs. (*C*) The legs of a microrobot are selectively folded as the acoustic excitation voltage is gradually increased to 40, 45, and 50 V_{PP}. The magenta dotted ellipse shows the folded leg. (*D*) Plot showing the dynamic folding of the microrobot's legs when tuning the acoustic excitation voltage against time. (*E*) A microrobot exhibits clockwise rotation in an acoustic field. As the excitation voltage increases, the microrobot shows a higher degree of contraction and exhibits a higher rotational speed. The blue curved arrow shows the rotational direction. (Scale bar [for all optical images], 100 μm.)

and various mechanical tests of living or non-living matter, such as fatigue testing (*SI Appendix*, Fig. S17). In the field of metamaterials, designs that incorporate acoustic-deformable microbeams facilitate complex 3D shape morphing and the creation of 2D-to-3D origami/kirigami microstructures. These structures can be used for optical guidance, acoustic guidance, and energy amplification, among other purposes. However, acoustic studies of these complex multi-element 3D microstructures could be computationally very demanding (*SI Appendix*, *Text S2*). In robotics, acoustically deformable beams open up novel micro-scale design paradigms and can enhance maneuverability by enabling functionalities such as steering, propulsion, and environmental adaptation. Furthermore, in flexible electronics, shape-transformable micromachines are beneficial for safe, portable, and friendly interactions, as well as for developing new functions. For medicine, as acoustic fields can easily extend into the body, these micromachines have the potential to dynamically navigate through complex blood vessels of varying sizes in the immediate future.

Our study shows exciting prospects across multiple scientific domains, but limitations currently exist. When multiple micromachines are simultaneously actuated in an acoustic field, micromachines tend to attract each other, leading to potential changes in their movement directions. This phenomenon is primarily caused by the strong secondary force of acoustic radiation resulting from the interaction of scattered waves between adjacent micromachines. However, the understanding of this complex acoustofluidic theory is incomplete. Different materials with varying acoustic impedances can be used to fabricate micromachines to fine-tune the secondary acoustic radiation force, enabling control over the attraction between micromachines. This approach also opens up possibilities for developing novel self-assembly mechanisms.

Materials and Methods

Photosensitive Mixture. The utilized photosensitive mixture is composed of a synthetic polymer (Polyethylene glycol with a molecular weight of 700, PEG 700, Sigma-Aldrich) and a photo-initiator (2-hydroxy-2-methyl-1-phenyl-propan-1-one, Darocur 1173, Sigma-Aldrich) at a ratio of 5:1. The photo-initiator will trigger the crosslink of PEG 700 when exposed to UV light. One droplet (~30 μL) of Rhodamine B solution (Sigma-Aldrich) is added to the mixture (5 mL) to align the mask, and one droplet (~30 μL) of blue food dye is added to the solution to visualize the fabricated micromachines.

Fabrication Method. Our custom-built UV photopolymerization is developed on an inverted microscope (NIKON, Eclipse Ti). A UV lamp (Nikon Intensilight C-HFGI) and a shutter controller (Vincent Associates, VCM-D1) are connected to irradiate a high-resolution photomask (CAD/Art Services, Inc.) inserted into the field stop of the microscope. Then, ~30 μL of the photosensitive mixture is spread on the fabrication area of a glass substrate (24 × 60 × 0.15 mm), and then the mixture is flatted by a cover glass (24 × 24 × 0.15 mm). When the mask is irradiated, passed UV light is focused by a 20× objective to polymerize the photosensitive mixture. The exposure time varied in a range of 50 to 300 ms. Notably, if the UV exposure time is too short, the structures may fail to polymerize or be excessively soft and consequently break when exposed to high excitation voltages. Hereby one micromachine is produced according to the photomask pattern. Once a micromachine is fabricated, we move the microscope platform for the next fabrication. Finally, the microstructures are cleaned to remove any residual contaminants using isopropanol (IPA).

Acoustic Setup. The experimental setup is built on a thin glass substrate, and a circular piezoelectric transducer (27 × 0.54 mm, resonance frequency 4.6 kHz ± 4%, Murata 7BB-27-4L0) is affixed to the glass substrate using an epoxy resin (2-K-Epoxidkleber, UHU Schnellfest). A droplet containing 50 to 80 μL of deionized water is spread on the substrate and covered with a cover glass to serve as a thin liquid medium (with a thickness of 90 to 150 μm). The substrate is then mounted on an inverted microscope (Axiovert 200 M, ZEISS). An electronic function generator (AFG-3011C, Tektronix) and an amplifier (0 to 60 V_{PP}, 15× amplification, High Wave 3.2, Digitum-Elektronik) are connected to the transducer to generate sound waves with tuneable excitation frequencies and voltages.

Imaging and Analysis. The shape transformation of micromachines is recorded with a high-speed camera (Chronos 1.4, Kron Technologies) attached to the inverted microscope. Recording frame rates range from 50 to 32,668 frames per second (fps). Recorded footage is analyzed in ImageJ.

Data, Materials, and Software Availability. All study data are included in the article and/or supporting information.

ACKNOWLEDGMENTS. We thank Vincent Christopher Winderoll, Jannes Huber, and Sam Rahimi for their assistance with experiments. This project has received funding from the European Research Council (ERC) under the European Union's Horizon 2020 research and innovation programme grant agreement No. 853309 (SONOBOTS), Swiss NSF (SNSF) under the SNSF Project funding MINT 2022 grant agreement No. 213058, and ETH Research Grant, grant agreement No. ETH-08 20-1. Z.Z. acknowledges the financial support from the China Scholarship Council (202006210065).

Author affiliations: [a]Acoustic Robotics Systems Lab, Institute of Robotics and Intelligent Systems, Department of Mechanical and Process Engineering, ETH Zurich, Zurich CH-8803, Switzerland

1. S. Ryu, R. E. Pepper, M. Nagai, D. C. France, Vorticella: A protozoan for bio-inspired engineering. *Micromachines* **8**, 4 (2017).
2. S. Armon, M. S. Bull, A. Aranda-Diaz, M. Prakash, Ultrafast epithelial contractions provide insights into contraction speed limits and tissue integrity. *Proc. Natl. Acad. Sci. U.S.A.* **115**, E10333–E10341 (2018).
3. S. J. Jeon, A. W. Hauser, R. C. Hayward, Shape-morphing materials from stimuli-responsive hydrogel hybrids. *Acc. Chem. Res.* **50**, 161–169 (2017).
4. S. Chen, J. Chen, X. Zhang, Z. Y. Li, J. Li, Kirigami/origami: Unfolding the new regime of advanced 3D microfabrication/nanofabrication with "folding". *Light Sci. Appl.* **9**, 75 (2020).
5. H. Kim *et al.*, Shape morphing smart 3D actuator materials for micro soft robot. *Mater. Today* **41**, 243–269 (2020).
6. A. Kopitca, K. Latifi, Q. Zhou, Programmable assembly of particles on a Chladni plate. *Sci. Adv.* **7**, eabi7716 (2021).
7. M. Z. Miskin *et al.*, Electronically integrated, mass-manufactured, microscopic robots. *Nature* **584**, 557–561 (2020).
8. Y. Liu *et al.*, Ultrafast shape-reconfigurable chiral mechanical metamaterial based on prestressed bistable shells. *Adv. Funct. Mater.* **33**, 2300433 (2023).
9. H. Fu *et al.*, Morphable 3D mesostructures and microelectronic devices by multistable buckling mechanics. *Nat. Mater.* **17**, 268–276 (2018).
10. A. Rafsanjani, Y. Zhang, B. Liu, S. M. Rubinstein, K. Bertoldi, Kirigami skins make a simple soft actuator crawl. *Sci. Robot.* **3**, eaar755 (2018).
11. E. Siéfert, E. Reyssat, J. Bico, B. Roman, Bio-inspired pneumatic shape-morphing elastomers. *Nat. Mater.* **18**, 24–28 (2019).
12. T. J. Jones, E. Jambon-Puillet, J. Marthelot, P. T. Brun, Bubble casting soft robotics. *Nature* **599**, 229–233 (2021).
13. J. N. Rodriguez *et al.*, Shape-morphing composites with designed micro-architectures. *Sci. Rep.* **6**, 27933 (2016).
14. D. Kim *et al.*, Shape-memory effect in twisted ferroic nanocomposites. *Nat. Commun.* **14**, 750 (2023).
15. Y. Xia, Y. He, F. Zhang, Y. Liu, J. Leng, A review of shape memory polymers and composites: Mechanisms, materials, and applications. *Adv. Mater.* **33**, 1–33 (2021).
16. Y. Zhao *et al.*, Twisting for soft intelligent autonomous robot in unstructured environments. *Proc. Natl. Acad. Sci. U.S.A.* **119**, e2200265119 (2022).
17. K. Liu, F. Hacker, C. Daraio, Robotic surfaces with reversible, spatiotemporal control for shape morphing and object manipulation. *Sci. Robot.* **6**, eabf5116 (2021).
18. E. W. H. Jager, O. Inganäs, I. Lundström, Microrobots for micrometer-size objects in aqueous media: Potential tools for single-cell manipulation. *Science* **288**, 2335–2338 (2000).
19. E. Hajiesmaili, D. R. Clarke, Reconfigurable shape-morphing dielectric elastomers using spatially varying electric fields. *Nat. Commun.* **10**, 183 (2019).
20. E. Hajiesmaili, N. M. Larson, J. A. Lewis, D. R. Clarke, Programmed shape-morphing into complex target shapes using architected dielectric elastomer actuators. *Sci. Adv.* **8**, eabn9198 (2022).
21. H. Hu *et al.*, Editing the shape morphing of monocomponent natural polysaccharide hydrogel films. *Research* **2021**, 9786128 (2021).
22. Z. Zheng *et al.*, Ionic shape-morphing microrobotic end-effectors for environmentally adaptive targeting, releasing, and sampling. *Nat. Commun.* **12**, 411 (2021).
23. H. Zhang, X. Guo, J. Wu, D. Fang, Y. Zhang, Soft mechanical metamaterials with unusual swelling behavior and tunable stress-strain curves. *Sci. Adv.* **4**, eaar853 (2018).
24. C. Xin *et al.*, Environmentally adaptive shape-morphing microrobots for localized cancer cell treatment. *ACS Nano* **15**, 18048–18059 (2021).
25. Y. C. Cheng, H. C. Lu, X. Lee, H. Zeng, A. Priimagi, Kirigami-based light-induced shape-morphing and locomotion. *Adv. Mater.* **32**, 1906233 (2020).
26. J. A. Lv *et al.*, Photocontrol of fluid slugs in liquid crystal polymer microactuators. *Nature* **537**, 179–184 (2016).
27. Y. Chen *et al.*, Light-driven dandelion-inspired microfliers. *Nat. Commun.* **14**, 3036 (2023).
28. Y. Wang *et al.*, Light-activated shape morphing and light-tracking materials using biopolymer-based programmable photonic nanostructures. *Nat. Commun.* **12**, 1651 (2021).
29. Z. Zhang, D. Ahmed, Light-driven high-precision cell adhesion kinetics. *Light Sci. Appl.* **11**, 10–11 (2022).
30. D. Hwang, E. J. Barron, A. B. M. Tahidul Haque, M. D. Bartlett, Shape morphing mechanical metamaterials through reversible plasticity. *Sci. Robot.* **7**, eabg2171 (2022).
31. Z. Ding *et al.*, Direct 4D printing via active composite materials. *Sci. Adv.* **3**, e160289 (2017).
32. Z. Zheng *et al.*, Electrodeposited superhydrophilic-superhydrophobic composites for untethered multi-stimuli-responsive soft millirobots. *Adv. Sci.* **10**, 2302409 (2023).
33. Z. Zhao *et al.*, Digital printing of shape-morphing natural materials. *Proc. Natl. Acad. Sci. U.S.A.* **118**, e2113715118 (2021).
34. J. Cui *et al.*, Nanomagnetic encoding of shape-morphing micromachines. *Nature* **575**, 164–168 (2019).
35. Y. Alapan, A. C. Karacakol, S. N. Guzelhan, I. Isik, M. Sitti, Reprogrammable shape morphing of magnetic soft machines. *Sci. Adv.* **6**, eabc6414 (2020).
36. N. Xia *et al.*, Dynamic morphological transformations in soft architected materials via buckling instability encoded heterogeneous magnetization. *Nat. Commun.* **13**, 7514 (2022).
37. H. Gu, Q. Boehler, D. Ahmed, B. J. Nelson, Magnetic quadrupole assemblies with arbitrary shapes and magnetizations. *Sci. Robot.* **4**, eaax8977 (2019).
38. Y. Kim, H. Yuk, R. Zhao, S. A. Chester, X. Zhao, Printing ferromagnetic domains for untethered fast-transforming soft materials. *Nature* **558**, 274–279 (2018).
39. S. Wu *et al.*, Symmetry-breaking actuation mechanism for soft robotics and active metamaterials. *ACS Appl. Mater. Interfaces* **11**, 41649–41658 (2019).
40. X. Ni *et al.*, Soft shape-programmable surfaces by fast electromagnetic actuation of liquid metal networks. *Nat. Commun.* **13**, 5576 (2022).
41. Y. Bai *et al.*, A dynamically reprogrammable surface with self-evolving shape morphing. *Nature* **609**, 701–708 (2022).
42. G. Mao *et al.*, Soft electromagnetic actuators. *Sci. Adv.* **6**, eabc0251 (2020).
43. J. J. Abbott, Z. Nagy, F. Beyeler, B. J. Nelson, Robotics in the small. *IEEE Robot. Autom. Mag.* **14**, 92–103 (2007).
44. M. Wautelet, Scaling laws in the macro-, micro- and nanoworlds. *Eur. J. Phys.* **22**, 601–611 (2001).
45. E. M. Purcell, Life at low Reynolds number. *Am. J. Phys.* **45**, 3–11 (1977).
46. Z. P. Bažant, "Asymptotic analysis of size effect" *in Scaling of Structural Strength*, Z. P. Bažant, Ed. (Elsevier, 2005), pp. 21–52.
47. M. Kaynak, A. Dolev, M. S. Sakar, 3D printed acoustically programmable soft microactuators. *Soft Robot.* **10**, 246–257 (2022).
48. Z. Zhang, A. Sukhov, J. Harting, P. Malgaretti, D. Ahmed, Rolling microswarms along acoustic virtual walls. *Nat. Commun.* **13**, 7347 (2022).
49. S. Yang *et al.*, Harmonic acoustics for dynamic and selective particle manipulation. *Nat. Mater.* **21**, 540–546 (2022).
50. J. Durrer *et al.*, A robot-assisted acoustofluidic end effector. *Nat. Commun.* **13**, 6370 (2022).
51. C. Wang *et al.*, Bioadhesive ultrasound for long-term continuous imaging of diverse organs. *Science* **377**, 517–523 (2022).
52. V. M. Jooss, J. S. Bolten, J. Huwyler, D. Ahmed, In vivo acoustic manipulation of microparticles in zebrafish embryos. *Sci. Adv.* **8**, eabm2785 (2022).
53. H. Hu *et al.*, A wearable cardiac ultrasound imager. *Nature* **613**, 667–675 (2023).
54. Y. Deng, A. Paskert, Z. Zhang, R. Wittkowski, D. Ahmed, An acoustically controlled helical microrobot. *Sci. Adv.* **9**, eadh526 (2023).
55. A. Ozcelik *et al.*, Acoustic tweezers for the life sciences. *Nat. Methods* **15**, 1021–1028 (2018).
56. A. Marzo, B. W. Drinkwater, Holographic acoustic tweezers. *Proc. Natl. Acad. Sci. U.S.A.* **116**, 84–89 (2019).
57. A. Del Campo Fonseca *et al.*, Ultrasound trapping and navigation of microrobots in the mouse brain vasculature. *Nat. Commun.* **14**, 5889 (2023).

58. Y. Song *et al.*, Wireless battery-free wearable sweat sensor powered by human motion. *Sci. Adv.* **6**, eaay9842 (2020).
59. D. Ahmed *et al.*, Selectively manipulable acoustic-powered microswimmers. *Sci. Rep.* **5**, 9744 (2015).
60. C. Dillinger, N. Nama, D. Ahmed, Ultrasound-activated ciliary bands for microrobotic systems inspired by starfish. *Nat. Commun.* **12**, 6455 (2021).
61. D. Dendukuri, D. C. Pregibon, J. Collins, T. A. Hatton, P. S. Doyle, Continuous-flow lithography for high-throughput microparticle synthesis. *Nat. Mater.* **5**, 365–369 (2006).
62. S. D. Danilov, M. A. Mironov, Mean force on a small sphere in a sound field in a viscous fluid. *J. Acoust. Soc. Am.* **107**, 143–153 (2000).
63. D. Ahmed *et al.*, Artificial swimmers propelled by acoustically activated flagella. *Nano Lett.* **16**, 4968–4974 (2016).
64. P. B. Muller, R. Barnkob, M. J. H. Jensen, H. Bruus, A numerical study of microparticle acoustophoresis driven by acoustic radiation forces and streaming-induced drag forces. *Lab Chip* **12**, 4617–4627 (2012).
65. J. T. Karlsen, H. Bruus, Forces acting on a small particle in an acoustical field in a thermoviscous fluid. *Phys. Rev. E–Stat. Nonlinear Soft Matter Phys.* **92**, 043010 (2015).
66. M. Settnes, H. Bruus, Forces acting on a small particle in an acoustical field in a viscous fluid. *Phys. Rev. E–Stat. Nonlinear Soft Matter Phys.* **85**, 016327 (2012).
67. D. Ahmed *et al.*, Bioinspired acousto-magnetic microswarm robots with upstream motility. *Nat. Mach. Intell.* **3**, 116–124 (2021).
68. Z. Zhang *et al.*, SonoRotor: An acoustic rotational robotic platform for zebrafish embryos and larvae. *IEEE Robot. Autom. Lett.* **8**, 2598–2605 (2023).
69. J. Janiak *et al.*, Acoustic microbubble propulsion, train-like assembly and cargo transport. *Nat. Commun.* **14**, 4705 (2023).